Diagnostics of Bar and End-Ring Connector Breakage Faults in Polyphase Induction Motors Through a Novel Dual Track of Time-Series Data Mining and Time-Stepping Coupled FE-State Space Modeling

Richard J. Povinelli, *Senior Member, IEEE*, John F. Bangura, *Member, IEEE*, Nabeel A. O. Demerdash, *Fellow, IEEE*, and Ronald H. Brown, *Member, IEEE*

***Abstract*—This paper develops the fundamental foundations of a technique for detection of faults in induction motors that is not based on the traditional Fourier transform frequency domain approach. The technique can extensively and economically characterize and predict faults from the induction machine adjustable speed drive design data. This is done through the development of dual-track proof-of-principle studies of fault simulation and identification. These studies are performed using our proven Time Stepping Coupled Finite Element-State Space method to generate fault case data. Then, the fault cases are classified by their inherent characteristics, so-called "signatures" or "fingerprints." These fault signatures are extracted or mined here from the fault case data using our novel Time Series Data Mining technique. The dual-track of generating fault data and mining fault signatures was tested here on three, six, and nine broken bar and broken end-ring connectors in a 208-volt, 60-Hz, 4-pole, 1.2-hp, squirrel cage 3-phase induction motor.**

***Index Terms*—Artificial intelligence, data mining, diagnostics through torque profiles, dynamical systems analysis, electric drives, fault diagnosis, induction motors, state space methods, time series, time stepping finite elements.**

I. Introduction

THREE-PHASE induction motors are presently in common use as the machine of choice in a majority of electronically controlled adjustable/variable speed drives (ASDs). During the past twenty years, there have been continuing efforts at studying and diagnosing of induction motor faults and associated performance characteristics [1]. As stated in [1] "performing reliable and accurate fault detection and diagnosis requires understanding the cause and effect of motor faults to motor performance." Accordingly, this paper demonstrates a method for detection of faults in induction machine adjustable speed drives (IMASDs).

Our approach to the problem of diagnosing faults in IMASDs is new and unique. First, we can generate data for a plethora of fault conditions by Time Stepping Coupled Finite Element-State Space (TSCFE-SS) [2]–[6] simulations without the need to encounter and acquire data for faults in actual field experience with IMASDs. Second, through Time Series Data Mining (TSDM) [7], [8] data searching for hidden patterns and nuances of differences between healthy performance and various fault signatures are automatically and efficiently carried out. These hidden patterns and nuances are made use of in fault identification.

This paper presents the development of the conceptual framework and proof-of-principle for a comprehensive set of algorithms for fault simulation, and fault identification/diagnosis in IMASDs. This proactive approach can head off the costly and catastrophic cascading of faults that lead to plant shutdowns and consequent long repair/maintenance periods. The resulting fault identification and diagnostic information also can facilitate the creation of efficient and effective maintenance schedules. The faulty operations include, but are not restricted to the following.

1) Broken bars and/or end-ring connectors in the squirrel-cages of induction motors [2].
2) Dynamic and static airgap eccentricities arising from assembly defects or subsequent mechanical/bearing problems that may develop in the field during operation [3].
3) Phase unbalances in stator armatures developing due to partial internal turn-to-turn short circuits, or phase unbalances resulting from unbalances in the inverter power electronic portion of a drive, or other phase voltage unbalances due to factors external to IMASD systems.

In this paper only the first type of these faults, namely broken squirrel-cage bars and end-ring connectors, are addressed.

The study of the effects of such faulty operations occurs through a dual track. The first track generates databases of fault signature profiles through TSCFE-SS simulation of healthy and faulty modes of operation of IMASDs [2]–[6]. The advantage of this method lies in its rigor in predicting effects of motor faults, that could include the incipient variety, on performance. The second track identifies and extracts hidden patterns and nuances that are characteristic and predictive of faults and incipient faults through TSDM [7], [8] of the fault signatures.

II. Time Stepping Coupled Finite Element-State Space Method

The TSCFE-SS technique computes on a time instant-by-instant basis the input phase and line currents, voltages, and de-

Manuscript received May 29, 2001.

R. J. Povinelli, N. A. O. Demerdash, and R. H. Brown are with the Department of Electrical and Computer Engineering, Marquette University, Milwaukee, WI 53201 USA (e-mail: richard.povinelli@marquette.edu, nabeel.demerdash@marquette.edu; ron.brown@marquette.edu).

J. F. Bangura is with Black & Decker, Baltimore, MD 21286 USA (e-mail: john.bangura@bdk.com).

Publisher Item Identifier S 0885-8969(02)01514-0.

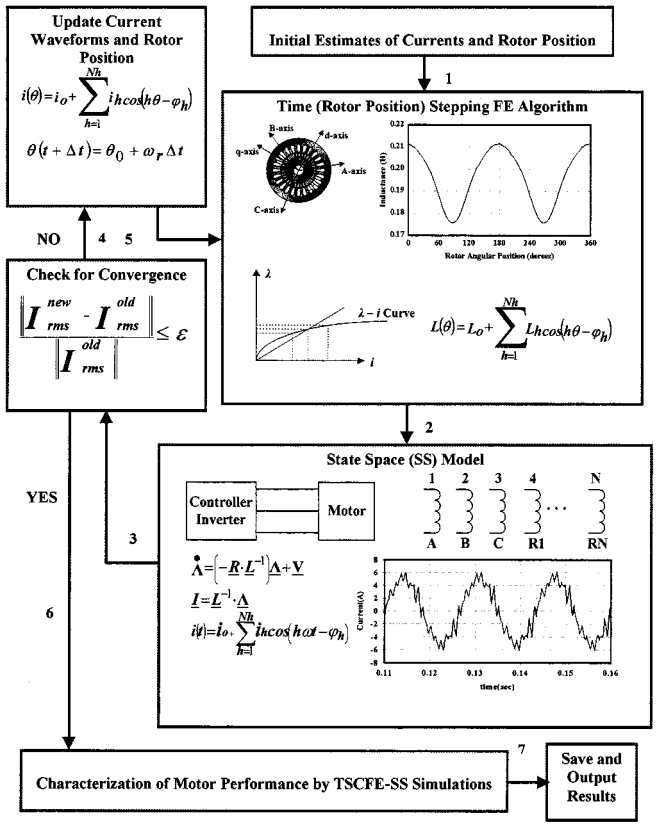

Fig. 1. Functional block-diagram/flow chart of the TSCFE-SS method.

veloped powers (torque) of a motor as functions of the particular magnetic circuit, winding layouts, and materials as well as inverter (power conditioner) operating conditions. Computations include ohmic and magnetic core losses as well as the effects due to modern fast electronic switching on overall motor-controller/drive interaction and resulting performance [6], [9]. Thus, the TSCFE-SS algorithms can also be used in parametric studies.

The TSCFE-SS model fully incorporates the nonlinear effects of magnetic saturation in the machine and makes full use of the natural machine winding's frame of reference [2]–[6]. (See Fig. 1 for the functional flow chart block diagram summarizing the essence of this approach.) Hence, this assures inclusion of all significant space harmonics due to the physical design and nonlinear nature of the motor, as well as the time harmonics generated from the inverter switching, in the motor-drive modeling and simulations. Accordingly, the simulated fault signatures are derived from time domain phase current, and voltage waveforms, as well as from simulated instantaneous torque profiles that rigorously incorporate the motors' design characteristics.

The validity of this simulation was verified by actual laboratory tests results on balanced sinusoidal three-phase, 208-volt (line-to-line) and inverter sources, which were reported in detail in [4]–[6], [10], and [11].

The TSCFE-SS algorithm was applied to the 1.2 hp, four-pole, 60 Hz case study motor, Fig. 2, to simulate two types of faults, first: three, six, and nine adjacent broken

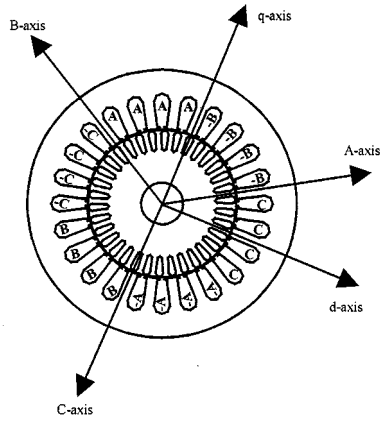

Fig. 2. Motor cross section.

squirrel-cage bars, and second: three, six, and nine adjacent broken squirrel-cage end-ring connectors.

The TSCFE-SS based model was used to generate the necessary database of motor current, voltage, and torque waveforms and profiles under healthy and faulty motor conditions, as will be detailed below in the section on applications and results.

III. Time Series Data Mining Method

The TSDM technique extracts fault signatures indicative of faults from the waveforms generated by the TSCFE-SS module. The TSDM method overcomes limitations (including stationarity and linearity requirements) of traditional time series analysis techniques by adapting data mining concepts for analyzing time series. Based soundly in dynamical systems theory [12], the TSDM method reveals hidden patterns in time series data. Here, the time series data are the current and voltage waveforms, as well as time-domain torque profiles.

A process called time-delay embedding [13] is used to transform the current waveforms and torque profiles (time series) into reconstructed state spaces, also called phase-spaces. Given the current time series, $I = \{i(k),\ k = 1\ldots, N\}$, where k is a time index, and N is the number of observations, a two-dimensional (2-D) phase-space is created by plotting $i(k-10)$ on the x–y plane's abscissa and $i(k)$ on the ordinate. Similarly, given the torque time series (time-domain torque profile), $T = \{\tau(k),\ k = 1, \ldots, N\}$, where again k is a time index, and N is the number of observations, a 2-D phase-space is created by plotting $\tau(k-10)$ on the x–y plane's abscissa and $\tau(k)$ on the ordinate.

In this investigation, this time delay embedding process was also applied to the time series of the torque first differences, $\Delta\tau(k) = \tau(k) - \tau(k-1)$. These results are presented in Section IV of applications.

Takens [12] proved that a reconstructed phase-space can be topologically equivalent to the original system state space. Given an original state space dimension d a sufficient condition for topological equivalence is that the reconstructed phase-space be dimensionally greater than $(d+1)$. We have also shown empirically in [7], [14], and [15] that characteristic features of a high dimensional system can be identified in low 2- or 3-D reconstructed phase-spaces.

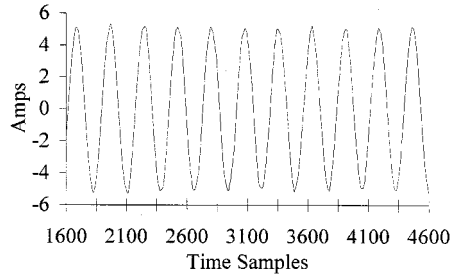

Fig. 3. Phase current for healthy motor.

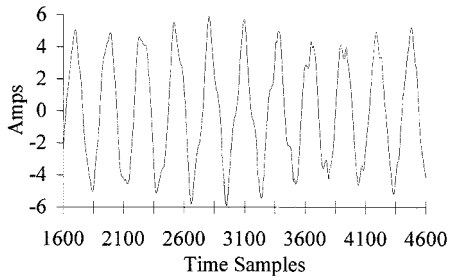

Fig. 4. Phase current for three broken bars.

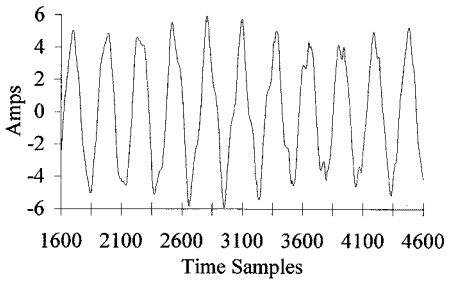

Fig. 5. Phase current for three broken connectors.

The feature used for distinguishing between reconstructed phase-spaces generated for different healthy and faulty modes of motor operation is the radius of gyration around the center of mass [16] of the points in the phase-space where each point in the phase-space is given a unit mass. The radius of gyration is calculated as follows:

$$r = \sqrt{\frac{\sum_{k=1+l}^{N} d(k)^2}{N-l}} \tag{1}$$

where

$$d(k)^2 = (x(k) - \mu_0)^2 + (x(k-l) - \mu_l)^2 \tag{2}$$

$$\mu_m = \frac{\sum_{k=l+m}^{N-l+m} x(k)}{N-l}. \tag{3}$$

l is the time lag of the phase space, N is the number of observations, and $x(k)$ is the time series observation at time index k. The value $d(k)$ is the distance of the kth phase-space point from the center of mass of the phase-space points. Since we are using a 2-D phase-space, which is formed by plotting $x(k-1)$ on the x–y plane's abscissa and $x(k)$ on the ordinate, the square of the distance is calculated by summing the squares of the differences between the phase-space point's value in each dimension and its corresponding center of mass for that same dimension. The value μ_m is the center of mass for each phase-space dimension.

This feature is a sufficient first approximation of the phase-space to allow identification of all healthy and faulty modes of operation. The decision rule for determining the mode of operation is defined as follows:

$$\text{index}(\min\{|r_1 - r_u|, |r_2 - r_u|, \ldots, |r_n - r_u|\}) \tag{4}$$

where, $r_1, r_2, \ldots, r_n$ are the radii of gyration of the known modes, r_u is the radius of gyration for the unknown mode, and the index operator returns the "index of the mode" with the closest radius of gyration to the unknown mode.

IV. Applications and Results

A. TSCFE-SS Simulations

The phase current waveforms for the healthy motor case and the cases with three broken bars as well as three broken connectors are given here in Figs. 3–5, respectively, (see [2], [9], and [11].

The modulation envelopes that appears in the current waveforms, Figs. 4 and 5, are due to the local heavy magnetic saturation appearing in locations within the rotor in the vicinity of bar/connector breakages. This heavy saturation is due to the absence of the demagnetizing effects of the rotor cage currents, which in normal healthy cages bucks the magnetizing effect of the stator mmf in these locations. A comparison between the healthy motor's flux plot Fig. 6 and the flux plot for the three broken bar case, Fig. 7, demonstrates this localized rotor saturation phenomenon surrounding the region housing the broken bars.

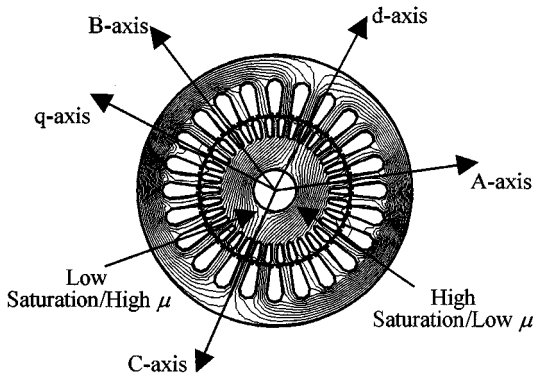

Fig. 6. Flux plot indicating the magnetically-induced "apparent saliency" effect.

The time-delay embedding process, described above, was applied to these phase current time series for the healthy, 3-broken bar, and 3-broken connector cases, and the resulting phase space plots are given in Figs. 8–10.

On a one-to-one correspondence basis, the reader can distinctly see a difference in pattern between the healthy cage case of Fig. 8 and the two faulty cage cases of Figs. 9 and 10. However, a distinction between the patterns of the phase-space for the three broken bars, Fig. 9 and the phase-space for the three broken connectors, Fig. 10 is not at once obvious.

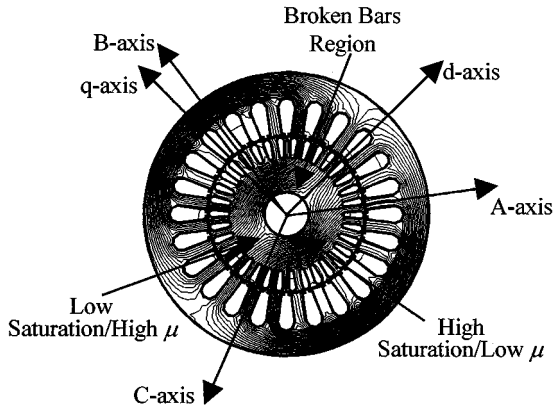

Fig. 7. Flux plot for the case of three broken bars.

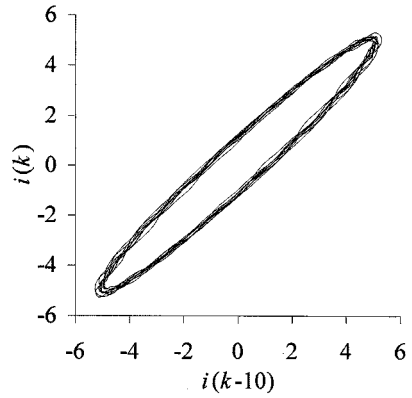

Fig. 8. Healthy motor current phase-space.

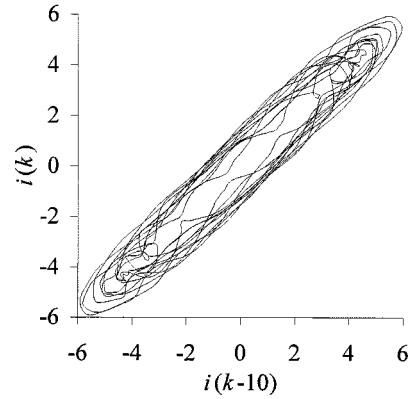

Fig. 9. Three broken bars current phase-space.

These authors found that such ambiguity between phase-space patterns is absent in the phase-space obtained from the time-domain torque profile first differences. Hence, the emphasis in this work from this point forward is placed on the time-domain torque profile first difference data.

The TSCFE-SS model simulation resulted in time-domain torque profiles [2], [11], for the healthy motor in Fig. 11, as well as the three, six, and, nine broken bar cases as given in Figs. 12–14, respectively. Meanwhile, the torque profiles for three, six, and nine broken connectors are given in Figs. 15–17, respectively.

Comparison of the healthy torque profile of Fig. 11 with an average torque value of 2.70 Nm, with the profiles of the three,

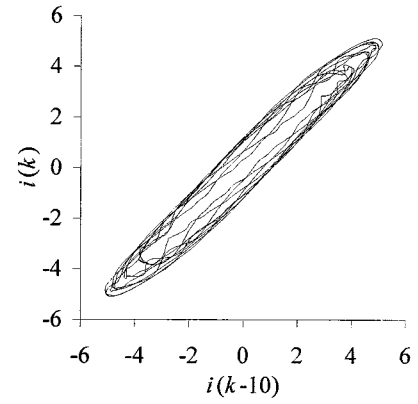

Fig. 10. Three broken connectors current phase-space.

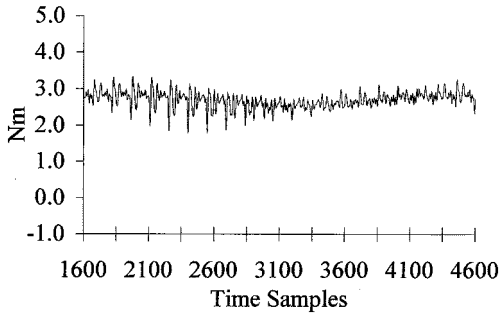

Fig. 11. Torque profile for the healthy motor.

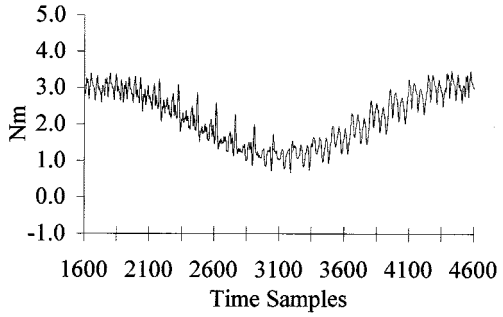

Fig. 12. Torque profile for three broken bars.

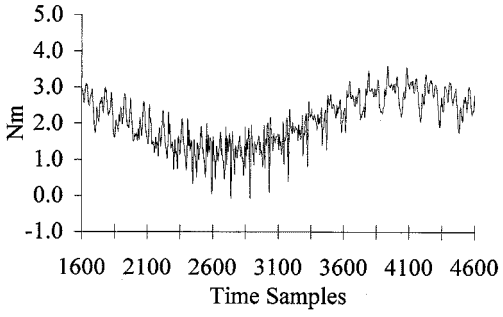

Fig. 13. Torque profile for six broken bars.

six, and nine broken bar cases in Figs. 12–14, with average torque values of 2.17, 2.07, and 2.12 Nm, respectively, reveals the degradation of developed torque averages. In addition, one cannot help but observe the worsening of torque ripple magnitudes and harmonic content. A similar comparison between the healthy motor torque profile of Fig. 11 with the three torque

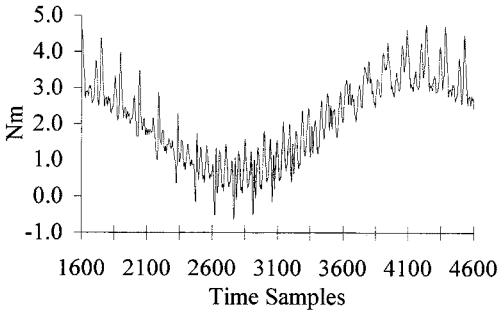

Fig. 14. Torque profile for nine broken bars.

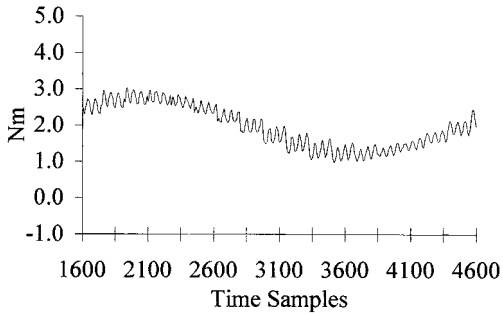

Fig. 15. Torque profile for three broken connectors.

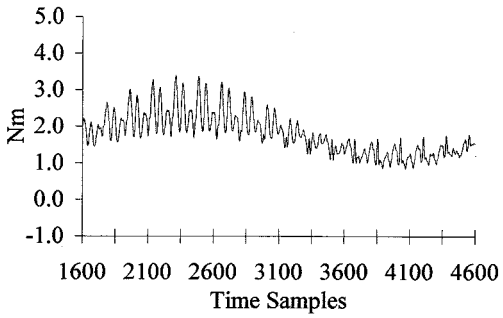

Fig. 16. Torque profile for six broken connectors.

profiles in Figs. 15–17, for the three, six, and nine broken connectors with torque averages of 1.96, 1.80, and 1.60 Nm, respectively, reveals the even more adverse (deleterious) global effect on the current flow in the cage that broken connectors have on the machine performance. This is revealed in the more dramatic average torque value degradations, and the quality of severe torque ripples. All these unhealthy cage cases reveal modulated envelopes resulting from localized rotor lamination saturation in the neighborhood of these breakages. Naturally, these localized breakage-associated saturation regions are traveling at the rotor speed, while the overall magnetic field pattern travels at the synchronous speed. This causes the resulting electromagnetic/electromechanical effects on the stator windings to reveal themselves in the waveforms and time-domain profiles at slip speed (slip frequency).

The time-delay embedding process summarized in Section III above was applied to these torque time series, and the resulting phase space plots will be shown and discussed in Section V of this paper.

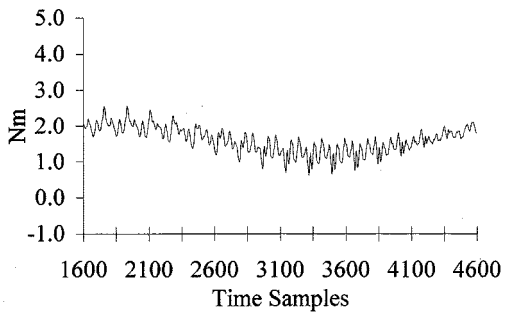

Fig. 17. Torque profile for nine broken connectors.

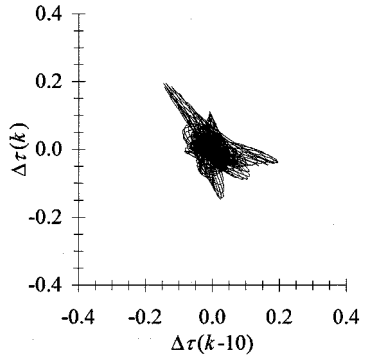

Fig. 18. Healthy motor torque first difference phase-space.

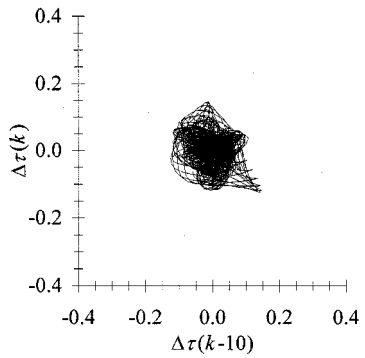

Fig. 19. Three broken bars torque first difference phase-space.

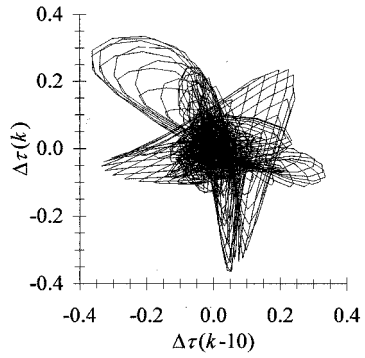

Fig. 20. Six broken bars torque first difference phase-space.

B. TSDM Fault Patterns

In this section, we present the results of the TSDM method for characterizing and identifying the various healthy and faulty

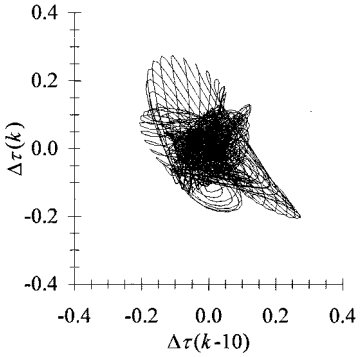

Fig. 21. Nine broken bars torque first difference phase-space.

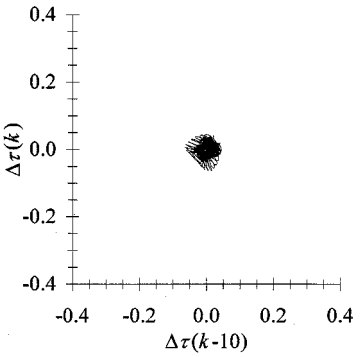

Fig. 22. Three broken connectors torque first difference phase-space.

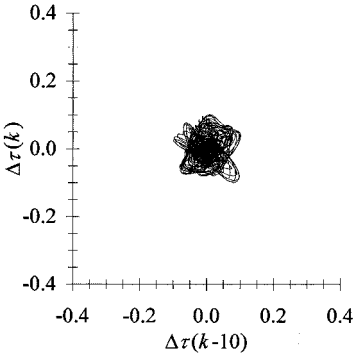

Fig. 23. Six broken connectors torque first difference phase-space.

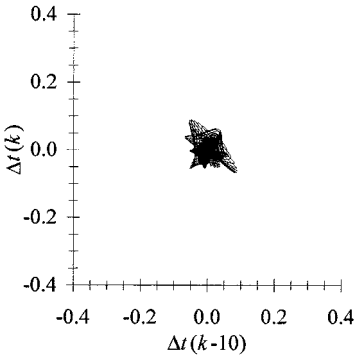

Fig. 24. Nine broken connectors torque first difference phase-space.

TABLE I
RADIUS OF GYRATION FOR TRANINING PHASE-SPACES

Operating Mode	Radius of Gyration
Healthy	0.0571
Three Broken Bars	0.0635
Six Broken Bars	0.1100
Nine Broken Bars	0.0999
Three Broken Connectors	0.0247
Six Broken Connectors	0.0432
Nine Broken Connectors	0.0346

TABLE II
RADIUS OF GYRATION FOR TESTING PHASE-SPACES

Operating Mode	Radius of Gyration
Healthy	0.0585
Three Broken Bars	0.0651
Six Broken Bars	0.1108
Nine Broken Bars	0.0994
Three Broken Connectors	0.0272
Six Broken Connectors	0.0441
Nine Broken Connectors	0.0348

modes of operation. To improve the ability to distinguish between the various modes of operation a torque first difference time series, $\Delta\tau(k) = \tau(k) - \tau(k-1)$, was generated from each of the seven torque time series of Figs. 11–17. Time-delay embedding was then applied to the torque first difference time series.

The resulting phase-space of the torque first difference time series is given for the healthy cage case in Fig. 18. Meanwhile, the phase-spaces for the three, six, and nine broken bar cases are given in Figs. 19–21, respectively. Also, the phase-spaces of the torque first difference for the three, six, and nine broken connector cases are given in Figs. 22–24, respectively. The distinction in shape between the seven torque first difference phase-spaces is strikingly obvious at first glance. This suggests that monitoring of motor torque for fault diagnosis and detection can be exploited as a powerful diagnostic tool, at least in critical motor drive systems.

The radius of gyration [16] for each phase-space is given in Table I. It is clear that the radius of gyration captures the differences between the various modes of operation that are clearly visible in Figs. 18–24. In this case study, all radii of gyration values for broken bars are greater than those for the healthy case, while all radii of gyration values for broken connectors are less than that for the healthy motor.

From the TSCFE-SS model we were able to obtain the time domain simulations for longer time duration than the one cycle time series shown in Figs. 11–17 for the torque profile. Thus, one easily obtains an "out-of-sample" or "test" torque first difference time series for each of the seven torque profile (torque first difference) cases analyzed by time delay embedding and radius of gyration calculations. Accordingly, the radius of gyration as a classifying feature was confirmed in the "out-of-sample" or "test" version of each motor mode of operation. The results are shown in Table II, and all compare well on a one to one correspondence with the values given in Table I, for each case, respectively.

TABLE III
ABSOLUTE DIFFERENCES BETWEEN TRAINING AND TESTING RADII OF GYRATION ($\times 10^{-2}$)

	H	B3	B6	B9	C3	C6	C9
H	**0.14**	0.80	5.37	4.24	2.99	0.65	2.22
B3	0.50	**0.16**	4.72	3.59	3.63	1.29	2.87
B6	5.15	4.49	**0.08**	1.06	8.28	5.94	7.52
B9	4.14	3.48	1.09	**0.04**	7.27	4.93	6.51
C3	3.38	4.04	8.61	7.48	**0.25**	2.59	1.02
C6	0.86	1.52	6.09	4.95	2.27	**0.07**	1.51
C9	3.99	2.98	11.6	7.99	1.24	1.33	**0.03**

The results of the classification algorithm are shown in Table III. The headings for the table are as follows: H—healthy motor, B3—three broken bars, B6—six broken bars, B9—nine broken bars, C3—three broken connectors, C6—six broken connectors, and C9—nine broken connectors, respectively. The actual mode of operation is given by the first column. The first row indicates the training radius of gyration that was used. The cells of the table are the Training radius of gyration (given by the column heading)—Testing radius of gyration (given by the row heading). The minimal difference in each row, and thus the classification, is bolded, and it confirms the validity of the approach, because of the small magnitudes of these bolded radii of gyration absolute differences.

In other words, the classification accuracy on the out-of-sample or testing data is 100%. Beyond the classification accuracy, the classifications are robust in the sense that for five of the seven classifications the next nearest class has absolute difference of radii of gyration that is one to two orders of magnitude greater than the correct class.

V. SUMMARY AND CONCLUSIONS

This work, which centered on the dual track utilization of TSCFE-SS modeling and TSDM techniques, to differentiate and identify various types of squirrel-cage breakages in induction motors has been shown in this paper to be a very promising approach for fault diagnostics. It was shown that time-domain motor torque profiles obtained from TSCFE-SS simulations, and their first differences can be phase transformed, and their corresponding phase transformations show distinct pattern differences for the healthy, three, six, and nine bar breakages. Furthermore, distinct difference exist between the healthy and three, six, and nine end ring connector breakages. The bar breakages and connector breakages can also be easily differentiated from each other. The concept of radius of gyration applied to the phase transformation of torque profiles also lead to an excellent quantification method for fault diagnostics. This approach appears to bear substantial promise for future expansion and use as a powerful fault identification and diagnostics tool in various motor drives. This approach could be integrated into a motor's adjustable speed drive electronics, and could be very useful in monitoring the health of key motor drives serving main auxiliary functions in power generation plants and similar industrial motor drives serving key functions.

REFERENCES

[1] M. E. H. Benbouzid, "Bibliography on induction motors faults detection and diagnosis," *IEEE Trans. Energy Conv.*, vol. 14, pp. 1065–1074, Dec. 1999.

[2] J. F. Bangura and N. A. Demerdash, "Diagnosis and characterization of effects of broken rotor bars and connectors in squirrel-cage induction motors by a time-stepping coupled finite element-state space modeling approach," *IEEE Trans. Energy Conv.*, vol. 14, pp. 1167–1175, Dec. 1999.

[3] ——, "Comparison between characterization and diagnosis of broken bars/end-ring connectors and airgap eccentricities of induction motors in ASDs using a coupled finite element-state space method," *IEEE Trans. Energy Conv.*, vol. 15, pp. 48–56, Mar. 2000.

[4] N. A. Demerdash and J. F. Bangura, "A time-stepping coupled finite element-state space modeling for analysis and performance quality assessment of induction motors in adjustable speed drives applications," presented at the Naval Symposium on Electric Machines, Newport, RI, 1997.

[5] N. A. O. Demerdash and J. F. Bangura, "Characterization of induction motors in adjustable-speed drives using a time-stepping coupled finite-element state-space method including experimental validation," *IEEE Trans. Ind. Applicat.*, vol. 35, pp. 790–802, July/Aug. 1999.

[6] J. F. Bangura and N. A. Demerdash, "Simulation of inverter-fed induction motor drives with pulse-width modulation by a time-stepping coupled finite element-flux linkage-based state space model," *IEEE Trans. Energy Conv.*, vol. 14, pp. 518–525, Sept. 1999.

[7] R. J. Povinelli and X. Feng, "Temporal pattern identification of time series data using pattern wavelets and genetic algorithms," presented at the Artificial Neural Networks in Engineering, St. Louis, MO, 1998.

[8] ——, "Data mining of multiple nonstationary time series," presented at the Artificial Neural Networks in Engineering, St. Louis, MO, 1999.

[9] J. F. Bangura and N. A. O. Demerdash, "Effects of broken bars/end-ring connectors and airgap eccentricities on ohmic and core losses of induction motors in ASDs using a coupled finite element-state space method," *IEEE Trans. Energy Conv.*, vol. 15, pp. 40–47, Mar. 2000.

[10] N. A. Demerdash, J. F. Bangura, F. N. Isaac, and A. A. Arkadan, "A time-stepping coupled finite-state-space model for induction motor drives-Part I: Model formulation and machine parameter computation & Part II: Machine performance computation and verification," *IEEE Trans. Energy Conv.*, vol. 14, pp. 1465–1478, Dec. 1999.

[11] J. F. Bangura, "A time-stepping coupled finite element-state space modeling for on-line diagnosis of squirrel-cage induction motor faults," Ph.D. dissertation, Marquette University, Milwaukee, WI, 1999.

[12] F. Takens, "Detecting strange attractors in turbulence," presented at the Dynamical Systems and Turbulence, Warwick, U.K., 1980.

[13] H. D. I. Abarbanel, *Analysis of Observed Chaotic Data*. New York: Springer, 1996.

[14] R. J. Povinelli, "Time series data mining: Identifying temporal patterns for characterization and prediction of time series events," Ph.D. dissertation, Marquette University, Milwaukee, WI, 1999.

[15] ——, "Characterization and prediction of welding droplet release using time series data mining," presented at the Artificial Neural Networks in Engineering, St. Louis, MO, 2000.

[16] P. A. Tipler, *Physics*, 2nd ed. New York: Worth, 1982, vol. 1.

Richard J. Povinelli (S'85–M'87–SM'01) received the B.S. degree in electrical engineering and the B.A. degree in psychology from the University of Illinois, Champaign-Urbana, the M.S. degree in computer and systems engineering from Rensselaer Polytechnic Institute, Troy, NY, and the Ph.D. degree in electrical and computer engineering from Marquette University, Milwaukee, WI, in 1987, 1989, and 1999, respectively.

From 1987 to 1990, he was a Software Engineer with General Electric Corporate Research and Development, Niskayuna, NY. From 1990 to 1994, he was with General Electric Medical Systems, Waukesha, WI, where he served as a Program Manager and then as a Global Project Leader. From 1995 to 1998, he held the positions of Lecturer and Adjunct Assistant Professor with the Department of Electrical and Computer Engineering, Marquette University, where, since 1999, he has been an Assistant Professor. His research interests include data mining of time series, chaos and dynamical systems, computational intelligence, and financial engineering.

Dr. Povinelli is a member of the Association for Computing Machinery, American Society of Engineering Education, Tau Beta Pi, Phi Beta Kappa, Sigma Xi, Eta Kappa Nu, Upsilon Pi Epsilon, and Golden Key.

John F. Bangura (S'96–M'99) received the B.S.E.E. degree from Clarkson University, Potsdam, NY, and the M.S.E.E. and Ph.D. degrees from Marquette University, Milwaukee, WI, in 1994, 1996, and 1999, respectively.

Currently, he is a Senior Engineer with Black & Decker, Baltimore, MD. His research interests include computational electromagnetics applied to electric machines and drives, modeling of dynamic performance of electric machines and drives, as well as condition monitoring and fault diagnosis of electric machinery drive systems.

Dr. Bangura is a member of the American Society of Engineering Education and of Sigma Xi.

Nabeel A. O. Demerdash (M'65–SM'74–F'90) received the B.S.E.E. degree (distinction with first-class honors) from Cairo University, Cairo, Egypt, and the M.S.E.E. and Ph.D. degrees from the University of Pittsburgh, Pittsburgh, PA, in 1964, 1967, and 1971, respectively.

From 1968 to 1972, he was a Development Engineer with the Large Rotating Apparatus Development Engineering Department, Westinghouse Electric Corporation, East Pittsburgh, PA. From 1972 to 1983, he held the positions of Assistant Professor, Associate Professor, and Professor in the Department of Electrical Engineering, Virginia Polytechnic Institute and State University, Blacksburg. From 1983 to August 1994, he held the position of Professor in the Department of Electrical and Computer Engineering, Clarkson University, Potsdam, NY. Since 1994, he has been a Professor in the Department of Electrical and Computer Engineering, Marquette University, Milwaukee, WI, in which he served as Department Chair from 1994 to 1997. He is the author or coauthor of more than 90 papers published in various IEEE journals. His research interests include power electronic applications to electric machines and drives, electromechanical propulsion and actuation, computational electromagnetics in machines and drives, as well as modeling of harmonic effects on machine-power systems dynamics.

Dr. Demerdash is active in the Electric Machinery Committee of the IEEE Power Engineering Society (PES) and its various subcommittees and is listed in the Distinguished Lecturer Program of the PES and the Distinguished Speaker Program of the IEEE Industrial Electronics Society. He is the winner of the 1999 IEEE Nikola Tesla Technical Field Award. He is also the winner of two 1994 Working Group Awards from both the PES and its Electric Machinery Committee and a winner of two 1993 Prize Paper Awards from both the PES and its Electric Machinery Committee. He is a member of the American Society of Engineering Education, Sigma Xi, and the Electromagnetics Academy.

Ronald H. Brown (M'72) received the B.S. degree in electrical engineering from The University of Illinois at Urbana-Champaign, the M.S. degree in electrical engineering from the University of Wisconsin-Madison, and the Ph.D. degree in electrical engineering from The University of Illinois at Urbana-Champaign, in 1976, 1977, and 1986, respectively.

He has been on the Faculty of Electrical and Computer Engineering at Marquette University, Milwaukee, WI, since 1985. He was at Bell Telephone Laboratories, Indianapolis, IN, and at Allen-Bradley Co., Milwaukee, WI, from 1978 to 1982. His research interests include nonlinear system identification, adaptive controls, prediction, and filtering, artificial neural control and artificial neural network training algorithms.